Supplement of Clim. Past, 21, 2561–2578, 2025
https://doi.org/10.5194/cp-21-2561-2025-supplement

Climate of the Past
Open Access
EGU

Supplement of

Distinct winter North Atlantic climate responses to tropical and extratropical eruptions over the last millennium in PMIP simulations and reconstructions

Qin Tao et al.

Correspondence to: Jesper Sjolte (jesper.sjolte@geol.lu.se)

S1. Selection of volcanic eruptions for the analysis of PMIP last millennium simulations

For the PMIP3 past1000 simulations, two ice core-based reconstructions of volcanic forcing, the Gao-Robock-Ammann (GRA) data (Gao et al., 2008) and the Crowley (CEA) data (Crowley and Unterman, 2013), have been used. The GRA data contains monthly sulfate aerosol loading at each 10° latitude band globally (Gao et al., 2008), while the CEA data provides stratospheric aerosol optical depth (AOD) at four latitude bands: 30°S–90°S, 0°–30°S, 0°–30°N, 30°N–90°N (Crowley and Unterman, 2013). Here, our analysis does not include the GISS-E2-R model because its past1000 simulations with the CEA and 2×GRA forcing have already been compared by Zambri et al. (2017). From the past1000 and past2k simulations in PMIP4 models, the eVolv2k volcanic forcing data with monthly AOD values at 96 latitudes globally has been used (Toohey and Sigl, 2017), including estimated date, source latitude, and amount of stratospheric sulfur injection for each eruption.

Since our main focus in this study is the volcanic impacts on winter North Atlantic climate, here we adapt the criterion suggested by Wang et al. (2023). We first calculate the maximum annual forcing over the extratropical Northern Hemisphere (30°N–90°N, with latitude-weighting) of the 1991 Pinatubo eruption in each forcing data set separately, then select the eruptions with maximum extratropical forcing no less than half of that from the 1991 Pinatubo eruption. For the eVolv2k data that does not cover the period of the 1991 Pinatubo eruption, we use the threshold (≥ 0.05) suggested by Wang et al. (2022, 2023) based on the CMIP6 volcanic forcing data for selection. To minimize potential interference between two events, we further exclude the eruptions occurring within five years of each other. However, if an eruption within this timeframe has the maximum extratropical forcing greater than that from the 1991 Pinatubo eruption, it is retained in the selection. Then, eruptions with source latitudes at 30°S–30°N are categorized as tropical eruptions (TROP), while those with source latitudes at 30°N–90°N are classified as Northern Hemisphere extratropical eruptions (NHET). The monthly aerosol forcing for each retained eruption is further examined to validate the selection. Overall, this screening procedure can also remove the TROP eruptions that predominantly spread towards the Southern Hemisphere, which may not influence the North Atlantic climate in the same way as the eruptions with a more symmetric latitudinal spread of aerosols. All selected eruptions during 851–1850 are listed in Table 2.

S2. Selection of volcanic eruptions for the analysis of paleoclimate reconstructions

For the SEA18v2 (Sjolte et al., 2018; Tao et al., 2023), ModE-RA (Valler et al., 2024), and EKF400v2 (Valler et al., 2021) reconstructions, we select 12 TROP eruptions with strengths exceeding that of the 1991 Pinatubo eruption (-6.49 W m^{-2}) and 8 NHET eruptions exceeding -1.8 W m^{-2} (Table 2) from the global volcanic aerosol forcing during the past 2500 years reconstructed by Sigl et al. (2015). Although this selection may not represent the most optimal subset for each individual reconstruction, it offers a consistent framework for comparing the overall post-volcanic responses across these three reconstructions.

This selection is based on the evaluation of how the choice of eruptions may affect the reconstructed climate. To assess this, the superposed epoch analysis is performed incrementally, starting with the largest event of each type of eruption and sequentially adding the next event in the descending order of forcing magnitude until all eruptions are included (Fig. S1a–f). The results indicate that the statistical significance of post-volcanic NAO change is sensitive to the number of eruptions included for analysis. In particular, the significance of NAO response after TROP eruptions in EKF400v2 shows a stronger dependency on event selection than in SEA18v2 and ModE-RA, likely due to its shorter temporal coverage and smaller number of eruptions it includes. Despite that, all three reconstructions consistently show an overall tendency toward a positive NAO phase after TROP eruptions and a negative NAO phase after NHET eruptions.

The analysis is then repeated but in ascending order of forcing magnitude (Fig. S1g–l), further highlighting the dominant influence of the largest eruptions. The NAO responses after TROP eruptions in SEA18v2 and ModE-RA, and the NAO responses after NHET eruptions in ModE-RA and EKF400v2 show a clear dominant effect from the very large eruptions. These results highlight the sensitivity in the detection of post-volcanic signals to the selection of volcanic eruptions, while increasing the number of events can reduce the uncertainty, the inclusion of small eruptions may dampen the composite signal (Bittner et al., 2016).

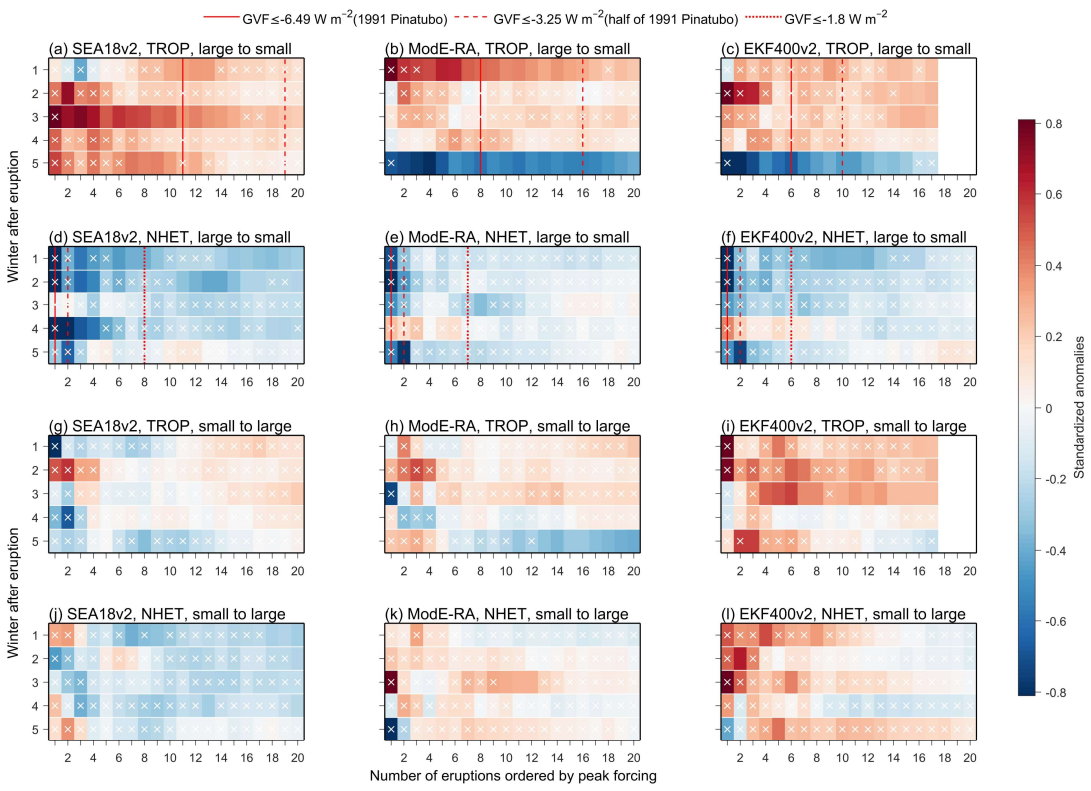

Figure S1. Responses of North Atlantic Oscillation (NAO) after tropical (TROP) and Northern Hemisphere extratropical (NHET) eruptions in three paleoclimate reconstructions. Winter NAO anomalies in the 5 years after TROP eruptions in (a) SEA18v2, (b) ModE-RA and (c) EKF400v2, with the order by adding eruptions from large to small peak forcing. (d-f) are the same as (a-c) but for NAO after NHET eruptions. (g-l) are the same as (a-f) but with the order by adding eruptions from small to large forcing. The three red reference lines indicate eruptions identified in the ice-core-based of global volcanic aerosol forcing (GVF) reconstructions (Sigl et al., 2015) with strengths exceeding that of the 1991 Pinatubo eruption (-6.49 W m^{-2}), half of Pinatubo's forcing (-3.25 W m^{-2}), and -1.8 W m^{-2}, respectively. Data that are not statistically significant at the 95% confidence level are marked with white crosses.

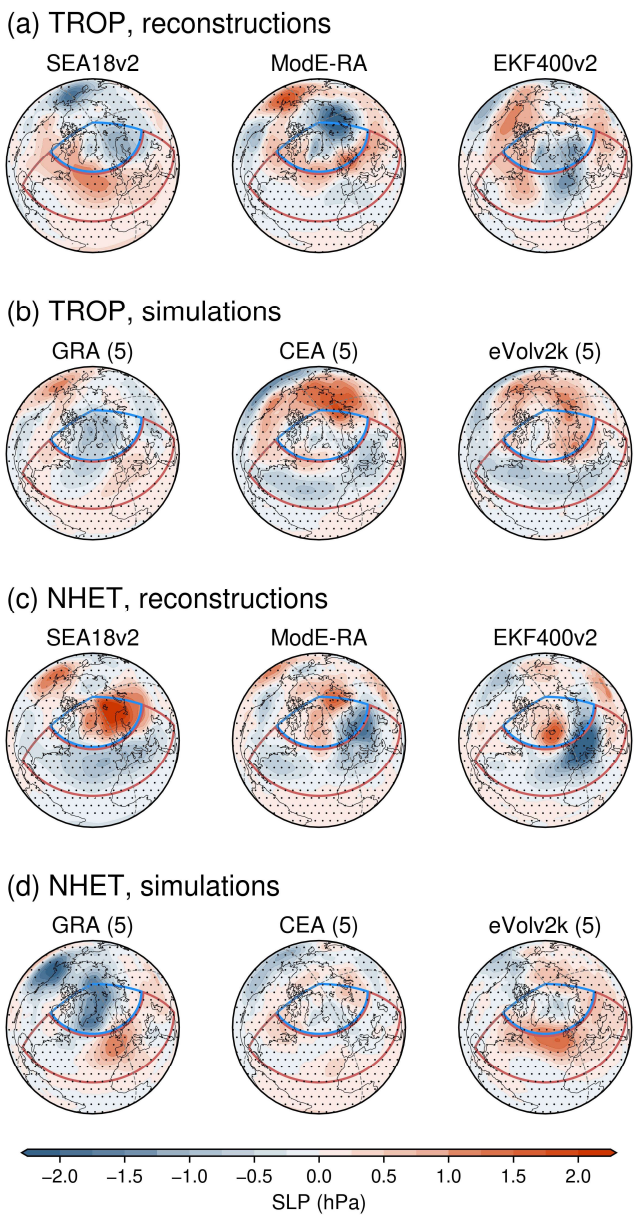

Figure S2. Spatial patterns of sea level pressure (SLP, units: hPa) anomalies in the second winter (December–February) following TROP and NHET volcanic eruptions. (a) SLP anomalies after TROP eruptions in three paleoclimate reconstructions (SEA18v2, ModE-RA, EKF400v2) and in (b) three multi-model ensemble means from PMIP simulations forced by GRA, CEA, and eVolv2k volcanic forcing datasets (numbers in brackets indicate the number of models forced by each dataset). (c–d) Same as (a–b), but for NHET eruptions. Anomalies are calculated relative to the mean conditions of the five years preceding the eruptions. Blue and red polygons (90°W–60°E, 55°N–90°N and 90°W–60°E, 20°N–55°N) are the two key regions of NAO (Stephenson et al., 2006). Black dots indicate regions where anomalies are not statistically significant at the 95% confidence level.

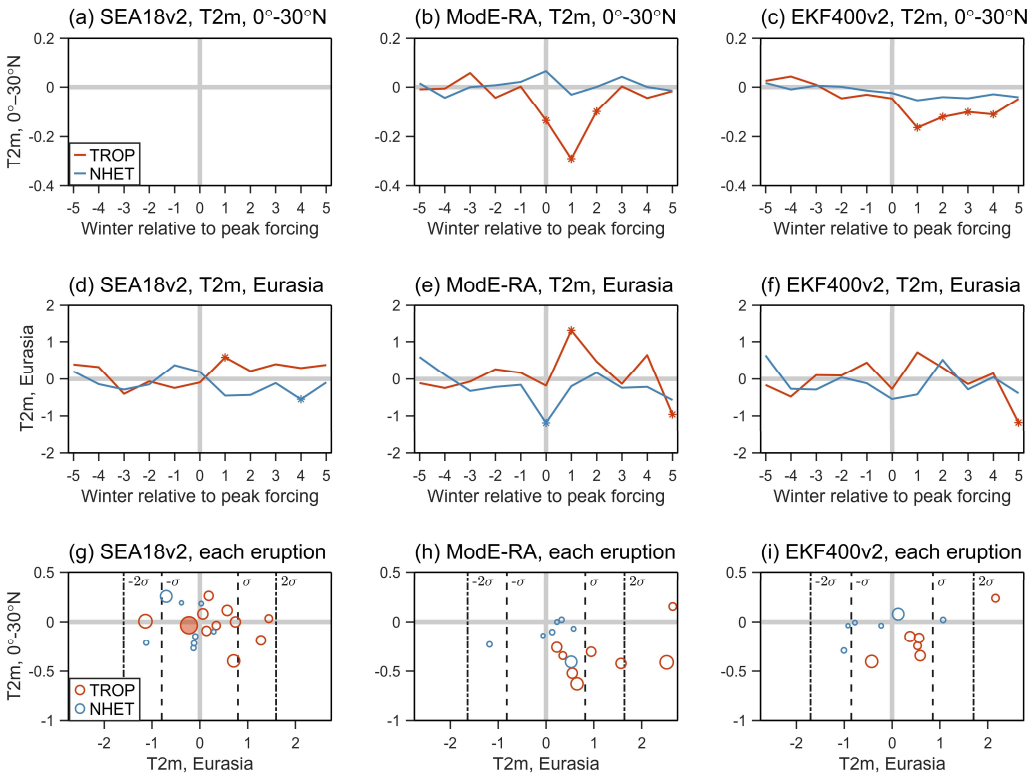

Figure S3. Superposed epoch analysis for near-surface air temperature (T2m, unit: °C) over 0°–30°N in (a) SEA18v2, (b) ModE-RA, and (c) EKF400v2 after TROP and NHET eruptions. Note that SEA18v2 only has reliable skills for the North Atlantic climate, so its results of T2m over 0°–30°N are omitted. (d-f) are the same as (a-c) but for the T2m over northern Eurasia (55°N–70°N, 10°E–120°E). Data statistically significant at the 95% confidence level are marked with asterisk. (g-i) are the T2m anomalies over 0°–30°N and northern Eurasia in the first winter after each eruption, relative to the mean of the reconstruction period. The dashed lines denote the ±σ and ±2σ of T2m changes over northern Eurasia over the last millennium. The sizes of the circles represent the magnitudes of the eruptions which are normalized to the Samalas eruption (the filled circle).

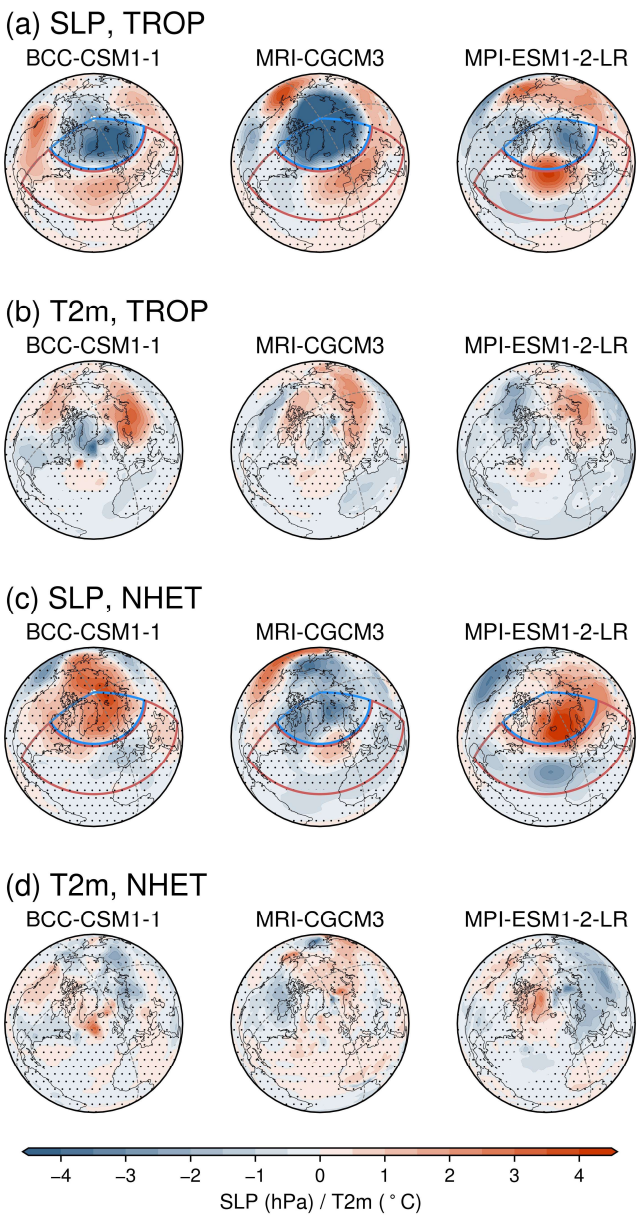

Figure S4. Spatial patterns of (a) SLP anomalies in BCC-CSM-1-1, MRI-CGCM3, and MPI-ESM1-2-LR during the first winter following TROP eruptions. (b) is the same as (a) but for T2m anomalies. (c-d) are the same as (a-b) but for the first winter after NHET eruptions. Blue and red polygons (90°W–60°E, 55°N–90°N and 90°W–60°E, 20°N–55°N) are the two key regions of NAO (Stephenson et al., 2006). Anomalies are computed relative to the average of five years before the eruptions. Black dots indicate regions where anomalies are not statistically significant at the 95% confidence level.

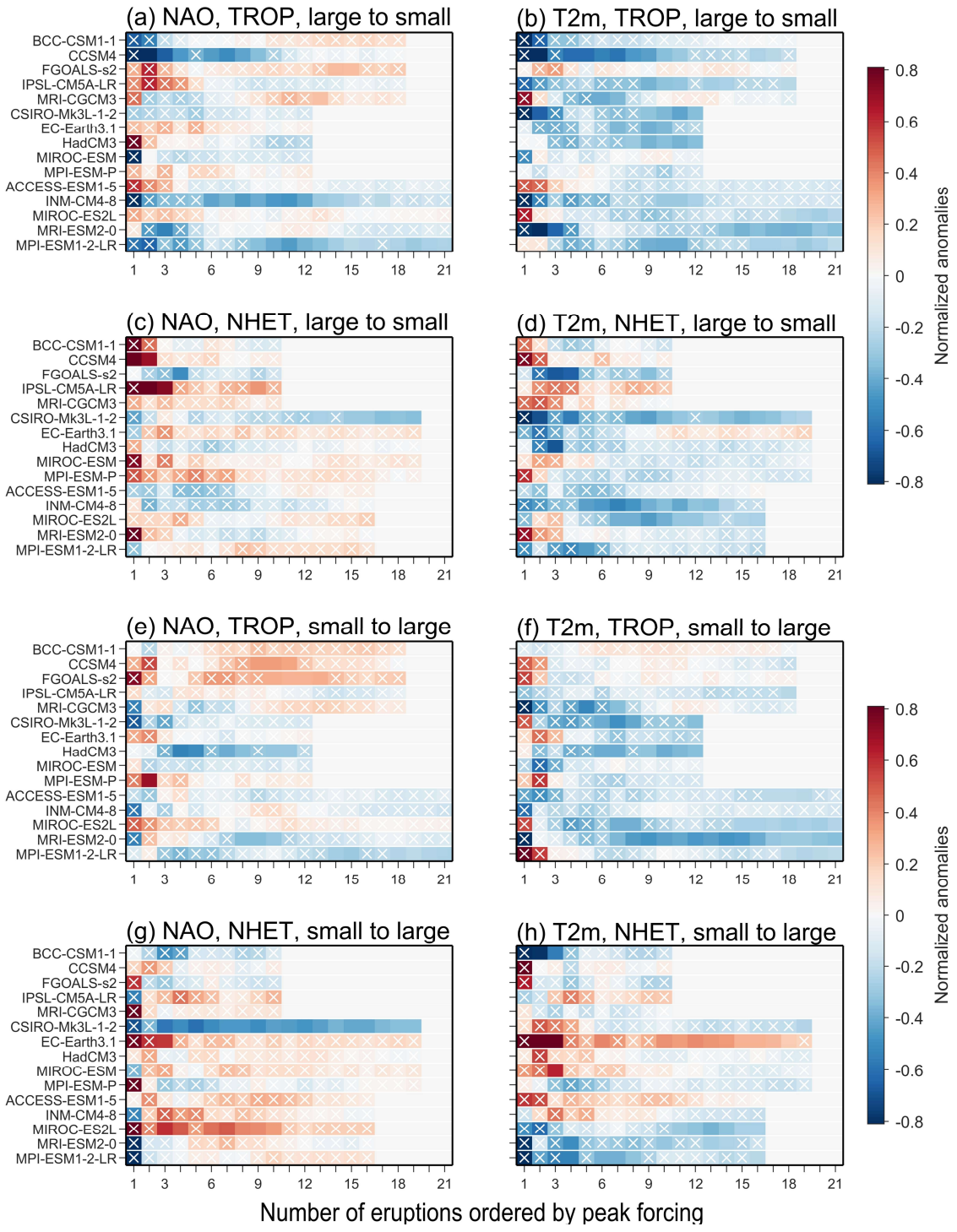

Figure S5. Responses of North Atlantic climate in the second winter to TROP and NHET eruptions in PMIP last millennium simulations. Results from superposed epoch analysis of (a) NAO indices and (b) T2m over northern Eurasia (55°N–70°N, 10°E–120°E) after TROP eruptions, with the order by adding eruptions from large to small peak forcing. (c-d) are the same as (a-b) but for NAO and T2m after NHET eruptions. (e-h) are the same as (a-d) but with the order by adding eruptions from small to large peak forcing. Data that are not statistically significant at the 95% confidence level are marked with white crosses.

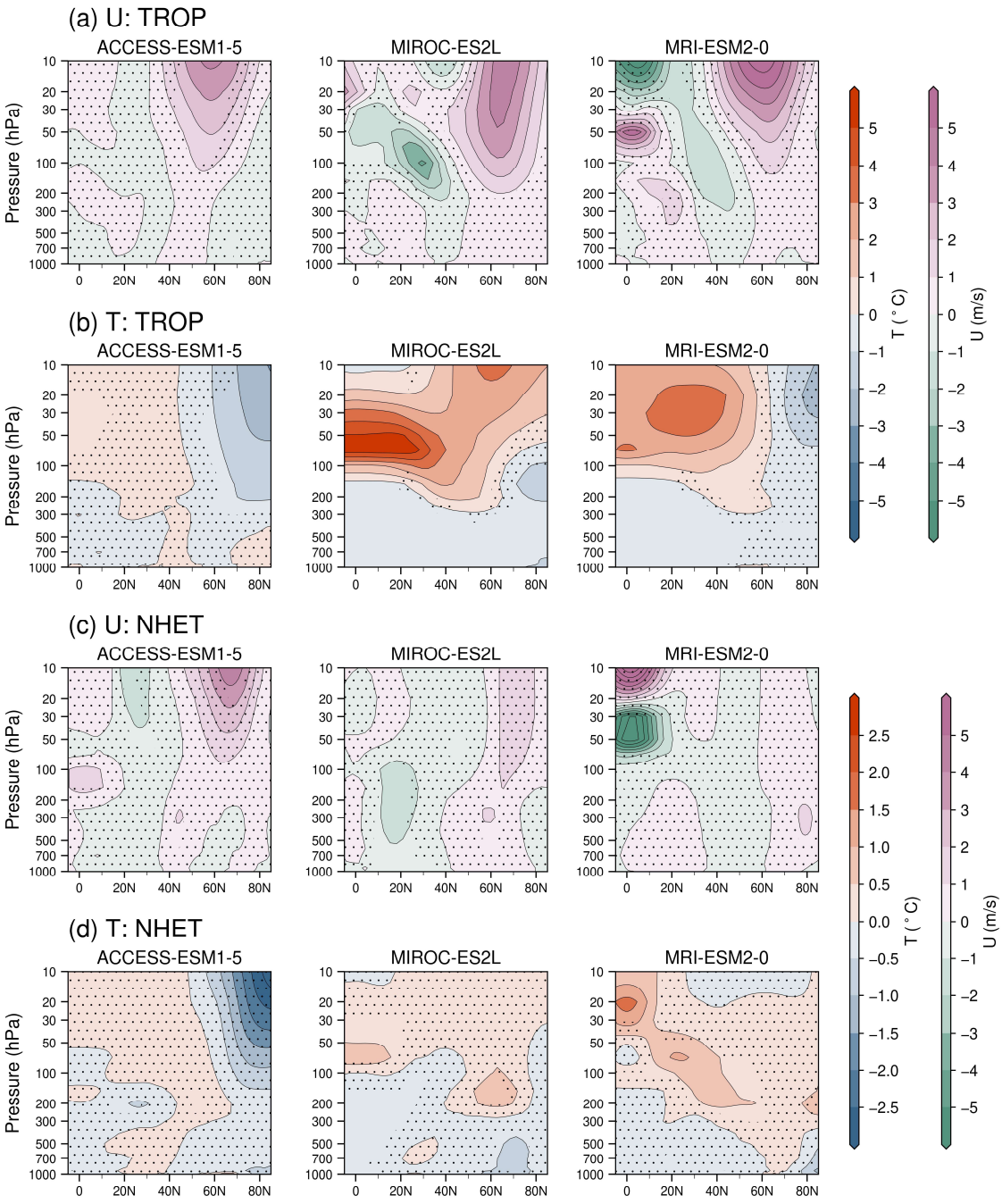

Figure S6. Northern Hemispheric zonal mean anomalies of (a) zonal wind (U, unit: m/s) and (b) air temperature (T, unit: °C) from the stratosphere to the troposphere in three eVolv2k-forced models during the first winter following TROP eruptions. (c-d) are the same as (a-b) but for NHET eruptions. Anomalies are computed relative to the average of five years before the eruptions. Black dots indicate regions where anomalies are not statistically significant at the 95% confidence level.

Table S1. List of key years for the selected TROP and NHET eruptions. Most events reach their maximum aerosol loading in the year following the onset of the eruption. For the few events peaking in the same year as the onset, the forcing data are typically assigned with onset in January, requiring the reference to be shifted to the subsequent winter to allow sufficient time for the climatic response to develop.

Volcanic forcing	TROP eruptions	NHET eruptions
GRA	871, 902, 993, 1002, 1082, 1123, 1168, 1196, 1228, 1259, 1285, 1453, 1601, 1642, 1762, 1810, 1816, 1836	934, 1177, 1329, 1460, 1585, 1720, 1730, 1756, 1784, 1832
CEA	897, 972, 1258*, 1287, 1331, 1442, 1601, 1674, 1810, 1816, 1832, 1836	875, 912, 925, 1061, 1068, 1101, 1119, 1313, 1389, 1460, 1516, 1526, 1554, 1586, 1668, 1732, 1740, 1784, 1797
eVolv2k	917, 977, 1029, 1109, 1172, 1192, 1231, 1258*, 1287, 1346, 1454, 1459, 1586, 1596, 1601, 1641, 1696, 1810, 1816, 1832, 1836	905, 940, 1021, 1183, 1201, 1211, 1330, 1478, 1511, 1568, 1647, 1668, 1730, 1740, 1767, 1784

* For the analysis of temperature anomalies following individual events, the Samalas eruption in the CEA and eVolv2k datasets is shifted to 1259, as most models forced with these datasets exhibit maximum tropical cooling during the 1258/1259 winter.

References

Bittner, M., Schmidt, H., Timmreck, C., and Sienz, F.: Using a large ensemble of simulations to assess the Northern Hemisphere stratospheric dynamical response to tropical volcanic eruptions and its uncertainty, Geophys Res Lett, 43, 9324–9332, https://doi.org/10.1002/2016GL070587, 2016.

Crowley, T. J. and Unterman, M. B.: Technical details concerning development of a 1200 yr proxy index for global volcanism, Earth Syst Sci Data, 5, 187–197, https://doi.org/10.5194/essd-5-187-2013, 2013.

Gao, C., Robock, A., and Ammann, C.: Volcanic forcing of climate over the past 1500 years: An improved ice core-based index for climate models, Journal of Geophysical Research: Atmospheres, 113, https://doi.org/10.1029/2008JD010239, 2008.

Sigl, M., Winstrup, M., McConnell, J. R., Welten, K. C., Plunkett, G., Ludlow, F., Büntgen, U., Caffee, M., Chellman, N., Dahl-Jensen, D., Fischer, H., Kipfstuhl, S., Kostick, C., Maselli, O. J., Mekhaldi, F., Mulvaney, R., Muscheler, R., Pasteris, D. R., Pilcher, J. R., Salzer, M., Schüpbach, S., Steffensen, J. P., Vinther, B. M., and Woodruff, T. E.: Timing and climate forcing of volcanic eruptions for the past 2,500 years, Nature, 523, 543–549, https://doi.org/10.1038/nature14565, 2015.

Sjolte, J., Sturm, C., Adolphi, F., Vinther, B. M., Werner, M., Lohmann, G., and Muscheler, R.: Solar and volcanic forcing of North Atlantic climate inferred from a process-based reconstruction, Climate of the Past, 14, 1179–1194, https://doi.org/10.5194/cp-14-1179-2018, 2018.

Stephenson, D. B., Pavan, V., Collins, M., Junge, M. M., and Quadrelli, R.: North Atlantic Oscillation response to transient greenhouse gas forcing and the impact on European winter climate: a CMIP2 multi-model assessment, Clim Dyn, 27, 401–420, https://doi.org/10.1007/s00382-006-0140-x, 2006.

Tao, Q., Sjolte, J., and Muscheler, R.: Persistent Model Biases in the Spatial Variability of Winter North Atlantic Atmospheric Circulation, Geophys Res Lett, 50, e2023GL105231, https://doi.org/10.1029/2023GL105231, 2023.

Toohey, M. and Sigl, M.: Volcanic stratospheric sulfur injections and aerosol optical depth from 500 BCE to 1900 CE, Earth Syst Sci Data, 9, 809–831, https://doi.org/10.5194/essd-9-809-2017, 2017.

Valler, V., Franke, J., Brugnara, Y., and Brönnimann, S.: An updated global atmospheric paleo-reanalysis covering the last 400 years, Geosci Data J, gdj3.121, https://doi.org/10.1002/gdj3.121, 2021.

Valler, V., Franke, J., Brugnara, Y., Samakinwa, E., Hand, R., Lundstad, E., Burgdorf, A.-M., Lipfert, L., Friedman, A. R., and Brönnimann, S.: ModE-RA: a global monthly paleo-reanalysis of the modern era 1421 to 2008, Sci Data, 11, 36, https://doi.org/10.1038/s41597-023-02733-8, 2024.

Wang, F., Arseneault, D., Boucher, É., Gennaretti, F., Yu, S., and Zhang, T.: Tropical volcanoes synchronize eastern Canada with Northern Hemisphere millennial temperature variability, Nat Commun, 13, 5042, https://doi.org/10.1038/s41467-022-32682-6, 2022.

Wang, F., Arseneault, D., Boucher, É., Gennaretti, F., Lapointe, F., Yu, S., and Francus, P.: Volcanic Imprints in Last-Millennium Land Summer Temperatures in the Circum–North Atlantic Area, J Clim, 36, 5923–5939, https://doi.org/10.1175/JCLI-D-23-0107.1, 2023.

Zambri, B., LeGrande, A. N., Robock, A., and Slawinska, J.: Northern Hemisphere winter warming and summer monsoon reduction after volcanic eruptions over the last millennium, Journal of Geophysical Research: Atmospheres, 122, 7971–7989, https://doi.org/10.1002/2017JD026728, 2017.